Cell, Vol. 113, 621–630, May 30, 2003, Copyright ©2003 by Cell Press

Solution Structure of a CUE-Ubiquitin Complex Reveals a Conserved Mode of Ubiquitin Binding

Richard S. Kang, Cynthia M. Daniels, Smitha A. Francis, Susan C. Shih, William J. Salerno, Linda Hicke, and Ishwar Radhakrishnan*

Department of Biochemistry, Molecular Biology, and Cell Biology
Northwestern University
Evanston, Illinois 60208

Summary

Monoubiquitination serves as a regulatory signal in a variety of cellular processes. Monoubiquitin signals are transmitted by binding to a small but rapidly expanding class of ubiquitin binding motifs. Several of these motifs, including the CUE domain, also promote intramolecular monoubiquitination. The solution structure of a CUE domain of the yeast Cue2 protein in complex with ubiquitin reveals intermolecular interactions involving conserved hydrophobic surfaces, including the Leu8-Ile44-Val70 patch on ubiquitin. The contact surface extends beyond this patch and encompasses Lys48, a site of polyubiquitin chain formation. This suggests an occlusion mechanism for inhibiting polyubiquitin chain formation during monoubiquitin signaling. The CUE domain shares a similar overall architecture with the UBA domain, which also contains a conserved hydrophobic patch. Comparative modeling suggests that the UBA domain interacts analogously with ubiquitin. The structure of the CUE-ubiquitin complex may thus serve as a paradigm for ubiquitin recognition and signaling by ubiquitin binding proteins.

Introduction

Ubiquitination is a key regulatory signal controlling protein activity and location. The covalent addition of ubiquitin to a specific lysine side chain(s) of a polypeptide substrate is accomplished by an elaborate machinery comprising, in general, a ubiquitin-activating enzyme, a ubiquitin-conjugating enzyme, and a ubiquitin ligase (Hershko and Ciechanover, 1998; Pickart, 2001; Weissman, 2001). The ubiquitin tag on the substrate can undergo additional rounds of ubiquitination to generate a chain of ubiquitin molecules linked by isopeptide bonds. A tetraubiquitin moiety serves as the minimum signal for efficient degradation of the substrate by the proteasome (Chau et al., 1989; Thrower et al., 2000).

Although selective protein degradation by the proteasome is a well-characterized function of ubiquitin, additional regulatory roles have been recently described. These include the sorting of proteins in the endocytic pathway (Hicke, 2001; Katzmann et al., 2002; Rotin et al., 2000), transcriptional activation and repression (Conaway et al., 2002; Muratani and Tansey, 2003), budding of retroviral virions (Pornillos et al., 2002), and intranuclear localization (Garcia-Higuera et al., 2001). Unlike proteasomal degradation, many of these processes rely on a monoubiquitin signal. Monoubiquitin signals appear to be transmitted through direct physical interactions with ubiquitin binding motifs found in eukaryotic proteins of diverse function. At least three such motifs have been well characterized thus far, including the UBA (*u*biquitin-*a*ssociated), UIM (*u*biquitin *i*nteracting *m*otif), and CUE (similar to a domain in the yeast Cue1 protein) motifs.

The UBA domain was the first ubiquitin binding motif to be described. The domain was identified through sequence database searches as a moderately-conserved, ~45 residue sequence found in a variety of proteins (Hofmann and Bucher, 1996). Because of its presence in a subset of both ubiquitinating and deubiquitinating enzymes, the domain was proposed to either bind ubiquitin or impose substrate specificity to these enzymes. UBA domains are also found in proteins involved in DNA repair such as Rad23, a variety of cellular kinases, and in adaptor proteins of AAA ATPase complexes. Several UBA domains were subsequently shown to bind monoubiquitin directly, albeit with moderate affinity (Bertolaet et al., 2001; Chen et al., 2001). Solution NMR structures of two UBA domains have been described, although not in complex with ubiquitin (Dieckmann et al., 1998; Mueller and Feigon, 2002).

The well-conserved 15 residue UIM motif was discovered based on the identification and characterization of a polyubiquitin binding sequence in the S5a subunit of the 19S proteasome regulatory complex (Young et al., 1998). The UIM motif is found in single or multiple copies in ubiquitin ligases and deubiquitinating enzymes and in multiple proteins involved in endocytosis and other cellular functions (Hofmann and Falquet, 2001). UIMs of several endocytic proteins have been shown to bind monoubiquitin with modest affinity (Polo et al., 2002; Raiborg et al., 2002; Shekhtman and Cowburn, 2002; Shih et al., 2002). Intriguingly, the UIMs of endocytic proteins have a role not only in binding monoubiquitinated targets including cell surface receptors, but also in promoting intramolecular monoubiquitination (Klapisz et al., 2002; Oldham et al., 2002; Polo et al., 2002).

A yeast two-hybrid screen for monoubiquitin-interacting proteins led to the identification of the CUE domain as a ubiquitin binding motif (Donaldson et al., 2003; Shih et al., 2003). Based on the molecular role of the Cue1 protein, the founding member of the family, the domain was proposed to recruit ubiquitin-conjugating enzymes (Biederer et al., 1997). However, genetic and biochemical studies suggest that CUE domains have a more general role as ubiquitin binding motifs (Donaldson et al., 2003; Shih et al., 2003). The CUE motif is a small, moderately-conserved domain of approximately 40 amino acid residues that is found in a variety of eukaryotic proteins (Ponting, 2000). CUE domain proteins include Vps9, a guanine nucleotide exchange factor that promotes vesicle fusion with endosomes; Tollip, an intermediate in interleukin-1 signaling; AMFR, a cytokine

*Correspondence: i-radhakrishnan@northwestern.edu

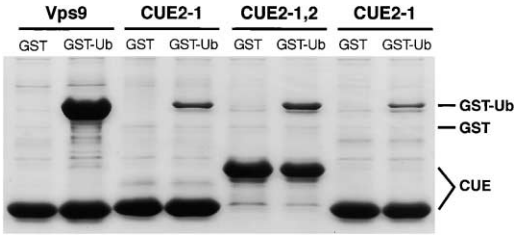

Figure 1. The CUE Domains of the Cue2 Protein Bind Ubiquitin Independently, But Not Cooperatively

Results of a ubiquitin binding assay conducted using His_6-tagged Vps9 (residues 408–450), CUE2-1 (Cue2 residues 8–50), CUE2-1,2 (Cue2 residues 8–97), and CUE2-2 (Cue2 residues 55–97). The assay was performed by immobilizing the His-tagged proteins onto a metal-affinity resin and incubating the proteins with *E. coli* lysates of GST or GST-ubiquitin. The bound proteins were eluted by boiling in sample buffer, resolved on an SDS-PAGE gel, and visualized by Coomassie staining.

receptor that regulates tumor cell motility and promotes metastasis; and AUP1, a ubiquitous protein involved in integrin signaling.

CUE domains, like UIMs, have a dual role in mono- and polyubiquitin recognition as well as in facilitating intramolecular monoubiquitination (Shih et al., 2003).

Despite the identification and characterization of multiple ubiquitin binding motifs, high-resolution information regarding the mode of recognition of monoubiquitin signals is not available. Ubiquitin interaction assays with UIM and CUE domains have provided intriguing hints, indicating that the domains may have a common mode of interaction with a hydrophobic patch on the ubiquitin surface (Beal et al., 1996; Shih et al., 2002, 2003). We present below the NMR structure of a CUE domain in complex with ubiquitin, which provides, to our knowledge, the first detailed insights into this interaction.

Results

Structure Determination of the CUE-Monoubiquitin Complex

The yeast Cue2 protein contains two copies of the CUE domain present in tandem near the amino terminus. Both copies of the CUE domain can bind monoubiquitin independently and belong to a subset of CUE domains that carry an MFP sequence and bind ubiquitin efficiently (Shih et al., 2003). To test whether these domains bind ubiquitin cooperatively, we incubated individual Cue2 CUE domains and a construct spanning both domains (henceforth designated CUE2-1, CUE2-2, and CUE2-1,2, respectively) with *E. coli* lysates containing GST or GST-ubiquitin. The Vps9 CUE domain, which binds ubiquitin efficiently, was included as a positive control (Shih et al., 2003). As expected, both CUE2-1 and CUE2-2 bound comparable amounts of ubiquitin (Figure 1). In comparison, CUE2-1,2 bound only a slightly greater amount of ubiquitin, implying that CUE2-1 and CUE2-2 bind ubiquitin independently, but not cooperatively. To gain insights into the mechanism of monoubiquitin recognition by CUE domains, we expressed and purified CUE2-1 and structurally characterized its interaction with yeast ubiquitin.

To assess the oligomerization properties of CUE2-1, we performed analytical ultracentrifugation studies over a broad range of loading concentrations (5–550 μM). Sedimentation equilibrium data were fitted with one- and two-component ideal models and a monomer-dimer equilibrium model. Satisfactory fits were obtained without invoking a self-association model. The predicted molecular weight (8158 Da) corresponded closely to the expected monomer molecular weight (8119 Da) of CUE2-1 (data not shown), indicating that the protein is monomeric over a wide range of concentrations.

NMR chemical shifts are exquisitely sensitive to the local electronic environment, and chemical shift perturbations are commonly used to monitor conformational changes and map intermolecular interfaces. Titrations of unlabeled CUE2-1 with ^{15}N-labeled ubiquitin led to significant but selective perturbation of amide proton and nitrogen resonances of a number of ubiquitin residues, implying a specific association between the two proteins. The residue with the most strongly perturbed amide chemical shifts is Lys48, the site of polyubiquitin chain formation (Figure 2A). The amide proton and nitrogen resonances shifted to new positions as a function of added CUE2-1, implying that the complex was dissociating and reassociating rapidly. From the binding isotherms of three nonneighboring ubiquitin residues (Leu8, Lys48, and Leu71), we calculated an average apparent K_D of 155 $\pm$ 9 μM, indicating that the CUE2-1-ubiquitin complex is modestly stable (Figure 2B).

The ^{1}H-^{15}N correlated spectrum of CUE2-1 was characterized by excellent dispersion of amide proton resonances, implying that the domain was folded in the absence of ubiquitin (Figure 3A). Significant changes occurred in the NMR spectrum of the CUE domain upon ubiquitin binding, but only a small number of resonances are perturbed. This pattern indicates a specific association mediated by a few select residues. The absence of large-scale changes in the NMR spectrum suggests that the CUE2-1 ubiquitin-interacting surface was already preformed. In spite of the modest affinity and fast dissociation kinetics, a number of intermolecular ^{1}H-^{1}H nuclear Overhauser effects (NOEs) were readily detected in the ^{13}C-filtered, ^{13}C-edited NOESY spectrum (Figure 3B), confirming a direct interaction.

The structure of the CUE2-1-ubiquitin complex was determined using NOE-based distance and chemical shift- and scalar coupling constant-based torsion angle restraints. Almost all intramolecular NOEs were assigned using an automated, iterative approach (Linge et al., 2003); intermolecular NOEs, on the other hand, were assigned iteratively and manually. An ensemble of 20 structures in excellent agreement with a large body of experimental data as indicated by low RMS differences with the input restraints, no distance or torsion angle violations greater than 0.3 Å and 5°, respectively, and good Ramachandran and convergence statistics (Table 1) was used for structural analysis.

Structure of the CUE2-1 Domain and Monoubiquitin in the Complex

The CUE2-1 domain is a compact globular domain comprising three short α helices arranged in a bundle (Figures 3A and 3B). The αA helix extends from His9 to

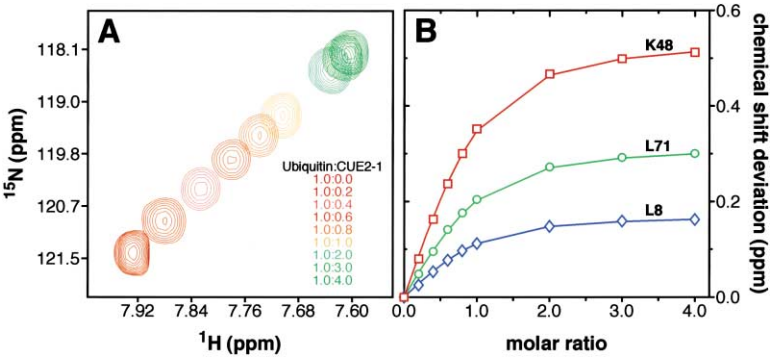

Figure 2. NMR Titrations of ^{15}N-Labeled Ubiquitin with Unlabeled CUE2-1

(A) Overlays of an expanded region from the ^{1}H-^{15}N correlated spectra of ^{15}N-ubiquitin showing changes in amide proton and nitrogen chemical shifts of Lys48 correlated with the amount of added CUE2-1. The peaks are colored from dark red (ubiquitin:CUE2-1 molar ratio 1:0) to dark green (molar ratio 1:4), with intermediate colors for the intermediate titration points.

(B) Weighted average chemical shift deviations Δ_{av} for three nonneighboring ubiquitin residues Lys48 (red), Leu71 (green), and Leu8 (blue), plotted as a function of added CUE2-1. The colored lines connect data points derived from the fitted functions.

Met19, while the αB and αC helices span residues Lys25–Glu34 and Leu39–Leu47, respectively (Figure 4B). The αA and αC helices are approximately coplanar and pack at an angle of 17° while simultaneously interacting with the intervening αB helix at an angle of 135°. Residues Leu13, Leu16, Leu28, Leu32, Thr42, Ile43, and

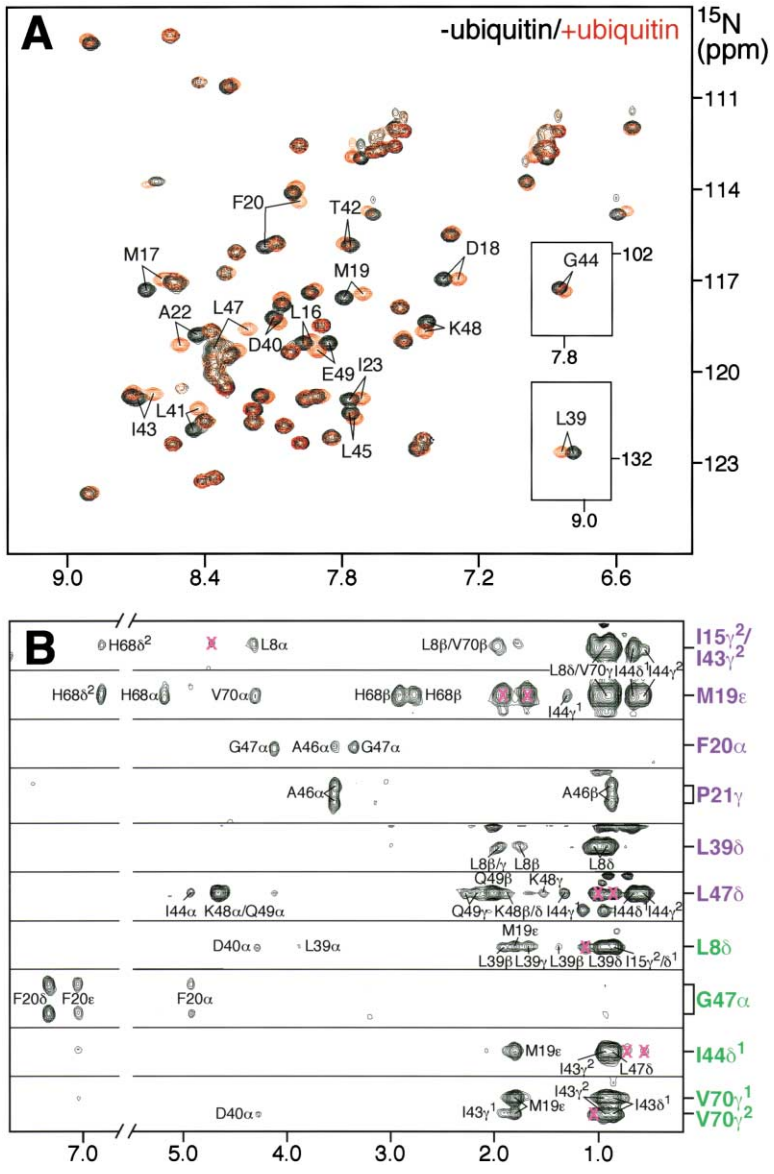

Figure 3. NMR Spectra of ^{15}N-Labeled CUE2-1 and a Subset of Intermolecular NOEs in the CUE-Ubiquitin Complex Demonstrating a Direct Interaction

(A) An overlay of the ^{1}H-^{15}N heteronuclear correlation spectra of ^{15}N-CUE2-1 in the absence (black) and in the presence (red) of an equivalent amount of unlabeled ubiquitin. The labels identify residues whose resonances are significantly perturbed.

(B) Selected strips from 3D ^{13}C-filtered, ^{13}C-edited NOESY spectra depicting intermolecular NOEs between CUE2-1 and ubiquitin. The labels identify ^{13}C bound protons of CUE2-1 (purple) and ubiquitin (green) that show NOEs to the corresponding ^{12}C bound protons of ubiquitin and CUE2-1, respectively (black). Incompletely suppressed signals from ^{13}C bound protons or other artifacts are denoted by X's.

Table 1. NMR Structure Determination Statistics	
Restraint Statistics	
Distance restraints	3328
Unambiguous NOE distance restraints	2560
Intraresidue	1311
Sequential [| i – j | = 1]	419
Medium-range [1 < | i – j | ≤ 4]	403
Intramolecular long range [| i – j | > 4]	273
Intermolecular	154
Hydrogen bonding distance restraints	90
Ambiguous NOE distance restraints	678
Torsion angle restraints	150 [69 ϕ, 69 ψ, 12 χ^1]
Ensemble Statistics for Structure Quality	
Restraint satisfaction	
Rms differences for distance restraints	0.010 ± 0.002 Å
Rms differences for torsion angle restraints	0.342 ± 0.020°
Deviations from ideal covalent geometry	
Bond lengths	0.002 ± 0.000 Å
Bond angles	0.340° ± 0.002°
Impropers	0.218° ± 0.004°
Ramachandran plot statistics[a]	
Residues in most favored regions	80.0%
Residues in allowed regions	18.8%
Residues in disallowed regions	1.2%
Average Atomic Rmsds from the Average Structure[a]	
All atoms [6–54 of CUE2-1 and 1–76 of ubiquitin]	1.88 Å
All atoms except disordered termini[b]	1.23 Å
Backbone atoms (N, C^α, C′)	
All residues [6–54 of CUE2-1 and 1–76 of ubiquitin]	1.41 Å
All residues excluding disordered termini[b]	0.62 Å
Secondary structural elements	0.55 Å

[a] Computed values do not include the 22 residue tag amino-terminal to CUE2-1.
[b] Disordered termini include residues 6–8 and 48–54 of CUE2-1 and 73–76 of ubiquitin.

Leu46 in the three helices, together with Phe20 and Ile23 in the loop connecting αA and αB helices, enclose a relatively small but well-defined hydrophobic core. Helices αB and αC are linked by a four-residue asparagine-rich loop in which the two central residues adopt unusual backbone conformations characterized by positive ϕ

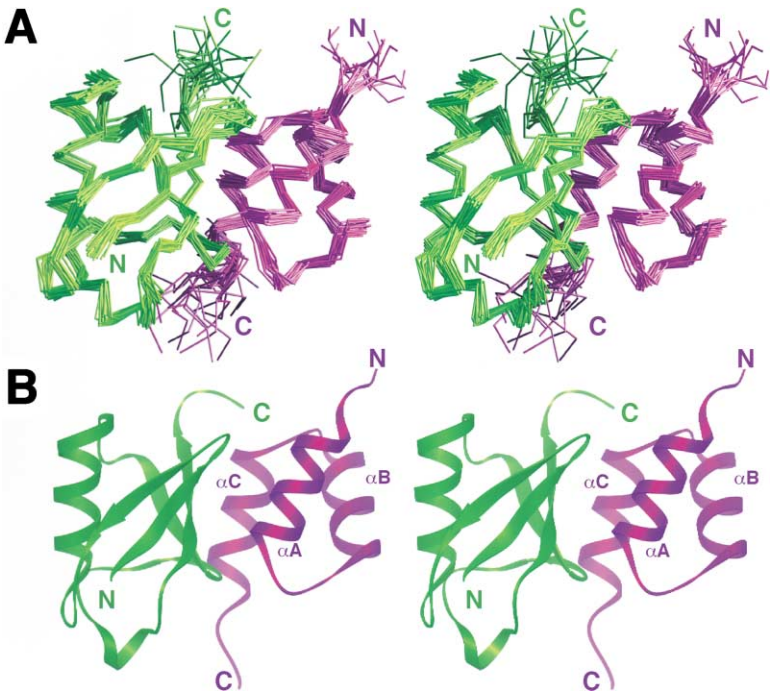

Figure 4. Solution Structure of the CUE2-1-Ubiquitin Complex

Stereo views of (A) the C^α trace of a best-fit superposition of backbone atoms in well-ordered regions (residues 9–47 of CUE2-1 and 1–72 of ubiquitin) of the ensemble of 20 NMR structures and (B) a ribbon diagram of a representative structure from the ensemble. CUE2-1 is colored in purple, and ubiquitin is shown in green.

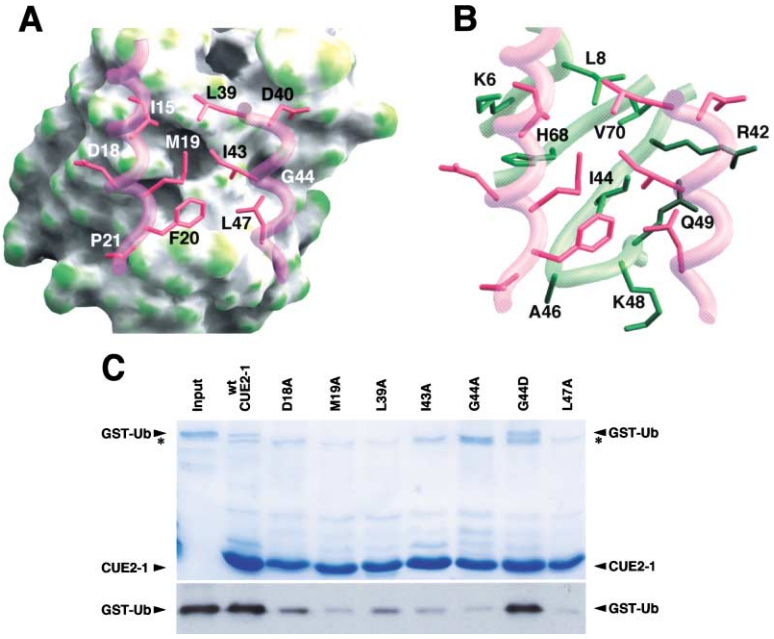

Figure 5. Noncovalent Interactions at the CUE2-1-Ubiquitin Interface and Contributions to the Overall Stability of the Complex

(A) A view of the molecular surface of ubiquitin is shown along with the side chains (magenta) of the interacting residues of CUE2-1. This view is rotated ~90° along the vertical axis relative to that shown in Figure 4. The molecular surface is color coded according to curvature (gray, concave; white, planar; and green, convex). The αA and αC helices of CUE2-1 (purple) are rendered semitransparently, while the αB helix is not shown for clarity.

(B) A similar view as that shown in (A) except the molecular surface of ubiquitin is replaced by a stick representation for the ubiquitin side chains (dark green) that interact with CUE2-1. The backbones of the interacting residues are shown in a worm representation (light green).

(C) Binding of His_6-CUE2-1 or His_6-CUE2-1 mutants to GST-ubiquitin in an in vitro pull-down assay. The asterisks identify a background band. Bound proteins were separated via SDS-PAGE and analyzed by Coomassie staining (top) or by an anti-GST antibody (bottom).

torsion angles. Overall, the backbone conformations are well defined except near the amino terminus, which includes the region corresponding to the nonnative 22 residue tag (data not shown), as well as the region immediately following the αC helix near the carboxy terminus (Figure 4A).

Ubiquitin adopts the well-characterized α + β ubiquitin fold comprising an α-helix and a five-stranded β sheet as the major structural elements. The structure of ubiquitin in the complex closely resembles that of the highest-resolution crystal structure of the free protein, as indicated by the low backbone rmsd of 1.16 Å for the segment extending from Met1–Arg72 (Vijay-Kumar et al., 1987). Differences between the crystal and NMR structures at the polypeptide backbone level are mainly confined to the loop regions linking secondary structural elements. Overall, the structure of ubiquitin is well defined except in the region spanning from Leu73–Gly76 at the carboxy terminus (Figure 4A). The poor definition of the structure in this region could be attributed to paucity of NMR restraints resulting from enhanced flexibility (Lee and Wand, 1999).

Noncovalent Interactions at the CUE2-1-Ubiquitin Interface

CUE2-1 binds mainly through the αA and αC helices to a surface defined in large part by the β1, β3, β4, and β5 strands of ubiquitin (Figures 3 and 4). The 17° packing angle between the αA and αC helices complements the natural twist associated with the ubiquitin β sheet. The intermolecular contacts cover a relatively small interface, about 400 $Å^2$ in each protein, which is consistent with the modest affinity of the interaction. A distinguishing feature of the ubiquitin surface in contact with CUE2-1 is a moderately deep hydrophobic pocket defined by the side chains of Leu8, Ile44, His68, and Val70 (Figure 5B). The pocket is filled by the side chain of Met19, a highly conserved residue in CUE domains that bind ubiquitin efficiently (Figures 4 and 5). The side chains of Ile15, Leu39, and Ile43 of CUE2-1 interact with the rim of this pocket, while those of Phe20, Pro21, and Leu47 propagate the hydrophobic contacts toward one edge of the β sheet and the turn region between β3 and β4 (Figures 4A and 4B). In so doing, the side chains interact with ubiquitin residues Ile44, Ala46, Gly47, and the aliphatic segments of Lys48 and Gln49 side chains (Figures 4A, 4B, and 5A). These interactions lead to the complete burial of the side chain of Ile44 (Figure 6A). This residue, analogous to Met19 of CUE2-1, fills a complementary pocket on the surface of the CUE domain.

In addition to the aforementioned hydrophobic interactions, the CUE2-1-ubiquitin complex appears to be stabilized by intermolecular electrostatic interactions. These were inferred using criteria including close proximity (<6 Å) of oppositely charged side chain moieties and the presence of such charge pairs in a majority of structures in the NMR ensemble. The side chains of Asp18 and Asp40 of CUE2-1 thus appear to engage Lys6 and Arg42 of ubiquitin, respectively, in electrostatic interactions (Figure 5B). Similar considerations also led to the identification of an intermolecular hydrogen bonding interaction between the backbone carbonyl and amide groups of Met19 and Gly47 of CUE2-1 and ubiquitin, respectively.

To evaluate the contributions made by individual CUE2-1 residues toward the stability of the CUE-ubiquitin complex, we mutated selected residues at the intermolecular interface in His_6-CUE2-1 to alanine and assayed these mutants immobilized on metal affinity beads for binding to GST-ubiquitin. As expected, mutation of Met19, Ile43, and Leu47—all highly conserved residues in the hydrophobic patch (Figures 4 and 6A)—abrogated ubiquitin binding (Figure 5C). Mutation of Asp18, Leu39, and Gly44 reduced ubiquitin binding relative to wild-type. Asp18 is involved in an electrostatic interaction with Lys6 of ubiquitin, while Leu39 contrib-

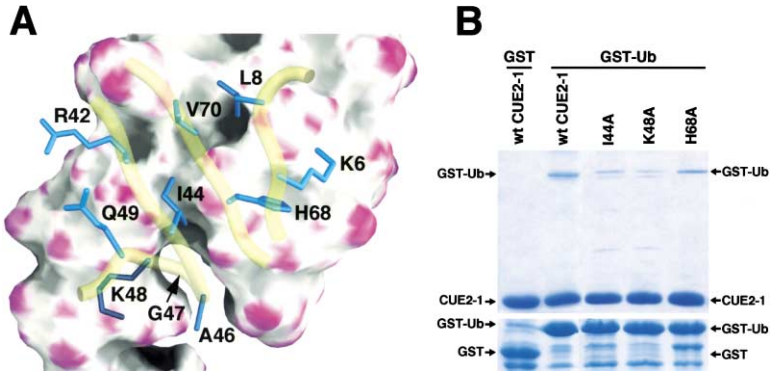

Figure 6. Intermolecular Interactions and Contributions to the Overall Stability of the CUE2-1-Ubiquitin Complex

(A) A view of the molecular surface of CUE2-1, color-coded according to curvature (gray, concave; white, planar; and magenta, convex), shown along with the interacting side chains (blue) of ubiquitin. The backbones of the interacting ubiquitin residues are shown in a worm representation (yellow).

(B) Binding of GST, GST-ubiquitin, or GST-ubiquitin mutants to His_6-CUE2-1. Bound proteins were resolved via SDS-PAGE and analyzed by Coomassie staining (top). The bottom shows the amount of GST or GST-ubiquitin used in these assays.

utes to the hydrophobic patch (Figure 5). Remarkably, mutation of Gly44 to an aspartate slightly enhanced ubiquitin binding relative to the wild-type protein (Figure 5C). Because of the proximity of this residue to Arg42 in ubiquitin, this suggests the likely acquisition of a favorable electrostatic interaction. Although Asp40 of CUE2-1 engages ubiquitin Arg42 in electrostatic interactions, a negatively charged residue at this position is absent in several CUE domains (Figure 7A). However, a negatively charged residue is present four residues carboxy-terminal to this position (i.e., corresponding to that of CUE2-1 Gly44) in these proteins, suggesting that residues at this position can mediate an equivalent or a more favorable interaction.

A complementary panel of GST-ubiquitin alanine point mutants was also tested for binding to His_6-CUE2-1 using the same assay described above. Predictably, the Ile44Ala mutation in ubiquitin had a strong destabilizing influence on the CUE2-1-ubiquitin interaction (Figure 6B). A comparable effect is also observed for the Lys48-Ala mutation, consistent with its role in engaging CUE2-1 in intermolecular interactions. The His68Ala mutant, on the other hand, retained comparable affinity as the wild-type protein, which is not inconsistent with its role in creating a hydrophobic pocket for the insertion of the CUE2-1 Met19 side chain.

Discussion

Posttranslational modifications such as phosphorylation, acetylation, and methylation have been implicated in signaling through mechanisms involving potentiation or disruption of protein-protein or protein-ligand interactions. The introduction of small chemical groups is sufficient in these cases to alter the conformational and physicochemical properties of the protein to profoundly influence function. In contrast, monoubiquitination introduces not only considerable bulk, but also a new molecular surface for protein-protein interaction. In the emerging view, a variety of ubiquitin binding motifs in diverse cellular proteins recognize the monoubiquitin signal independently of the modified protein substrate. Our studies of the CUE-ubiquitin interaction provide detailed insights into how the ubiquitin signal may be recognized by ubiquitin binding motifs in the cell.

Ubiquitin Recognition by CUE and UBA Domains

Biochemical and genetic analyses had previously implicated a hydrophobic patch defined by the side chains of Leu8, Ile44, and Val70 on the surface of ubiquitin as a key determinant for endocytosis and proteasomal degradation (Beal et al., 1996; Sloper-Mould et al., 2001).

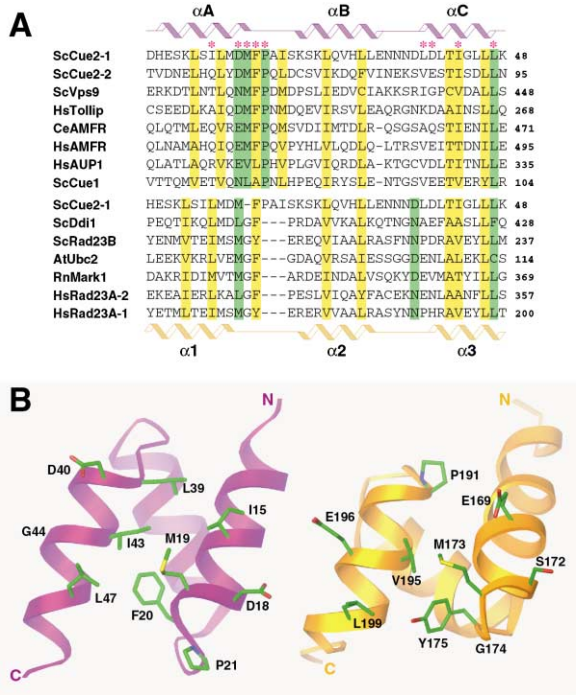

Figure 7. Sequence and Structural Similarity between the CUE and UBA Domains

(A) A multiple sequence alignment of CUE domains from a variety of proteins reproduced from the SMART (http://smart.embl-heidelberg.de) database (top). The asterisks identify residues in CUE2-1 that make direct contacts with ubiquitin. Conserved residues are highlighted; residues that contribute to the hydrophobic core are highlighted in yellow. A multiple sequence alignment of CUE2-1 with UBA domains, including those for which three-dimensional structures have been described (bottom). The cartoons at the top and bottom identify the locations of helices in the NMR structures of the yeast CUE2-1 and the human Rad23A UBA-1 domains, respectively. The alignment was guided by the structure of CUE2-1 and by the mode of interaction with ubiquitin. Species abbreviations are as follows: Sc, *S. cerevisiae*; Hs, *H. sapiens*; Ce, *C. elegans*; At, *A. thaliana*; and Rn, *R. norvegicus*.

(B) Side-by-side views of the CUE2-1 (left) and human Rad23A UBA-1 (right) domains. CUE2-1 residues involved in ubiquitin binding are shown. Equivalent residues in the UBA domain are also shown (right).

Protein-protein interaction assays conducted in vitro highlighted a role for this patch in ubiquitin binding by the UIM and CUE domains (Shih et al., 2002, 2003). The NMR structure of the CUE-ubiquitin complex confirms and extends these observations. The CUE domain not only engages residues within the hydrophobic patch, but also interacts with a ring of residues surrounding the patch (Figure 5). Intermolecular contacts are dominated by hydrophobic interactions between side chains of hydrophobic residues and between hydrophobic side chains and the aliphatic segments of charged or polar residues. Additional interactions including intermolecular electrostatic interactions at the periphery of the contact surface and a hydrogen bonding interaction also contribute toward the stability and specificity of the CUE-ubiquitin complex.

The CUE domain binding surface is a hydrophobic patch that is complementary to the ubiquitin hydrophobic surface. CUE domains contain two highly conserved sequence motifs including a MFP motif and a dileucine motif (Figure 7A), both of which were shown through mutational analyses to be functionally important for efficient interaction with ubiquitin (Shih et al., 2003). Residues in the MFP motif and the second leucine residue in the dileucine motif make significant contributions to the hydrophobic patch, whereas the phenylalanine and the first leucine residue are also involved in stabilizing the hydrophobic core of the domain, providing a straightforward explanation for the results from the mutational analyses. Interestingly, compared to the CUE domains from other proteins such as yeast Vps9 and Cue2, the Cue1 CUE domain exhibits significantly reduced affinity for ubiquitin (Shih et al., 2003). This can be readily explained by the strong deviations from the MFP consensus in the primary structure of the Cue1 CUE domain (Figure 7A). Although $\phi\phi$P (where ϕ is any bulky hydrophobic residue) may constitute a generalized motif for this segment, an MFP sequence is probably the most favorable from the standpoint of shape complementarity and packing efficiency. Based on the NMR structure of the CUE-ubiquitin complex, the CUE domains of all proteins listed in Figure 7A, with the exception of yeast Cue1 and to some extent human AUP1, appear to have all the necessary determinants for efficient interaction with ubiquitin.

To identify close structural relatives of the CUE domain, we searched the FSSP database using DALI (Holm and Sander, 1993). This led to the identification of the human Rad23A UBA-2 domain (PDB accession code 1DV0; Dieckmann et al., 1998) as the closest structural homolog of CUE2-1 based on a high value for the Z score of 3.6 and a low value for the atomic rmsd of 1.8 Å for the backbone C^{α} atoms. The CUE and UBA domains form compact, three-helix bundle structures and have many well-conserved residues, including several highly conserved hydrophobic residues at comparable positions (Figure 7A). The domains differ significantly in sequence length and composition in loop-1 that links the first and second helices. This translates into differences in helix packing geometries (Figure 7B). The highly conserved MFP motif in CUE domains is replaced by a similarly highly conserved MGF motif in the UBA domains. The invariant glycine in the MGF motif occupies a similar spatial position as the invariant proline in the MFP motif and is responsible for inducing a sharp turn that brings the methionine and the aromatic residue within the motif in close spatial proximity akin to the first two residues in the MFP motif in CUE domains.

Since the CUE and UBA domains share structural homology and because no high-resolution structure of UBA in complex with ubiquitin has yet been reported to our knowledge, we modeled the UBA-ubiquitin interaction based on the NMR structure of the CUE2-1-ubiquitin complex. We chose to model the interaction involving the human Rad23A UBA-1 domain (PDB accession code 1IFY; (Mueller and Feigon, 2002) rather than the UBA-2 domain because of its greater sequence similarity with CUE2-1. Although the manner in which the helices assemble within the respective domains is slightly different (Figure 7B), the set of determinants required to engage ubiquitin in a fashion analogous to the CUE domain appears to be surprisingly well conserved in the UBA domain. For example, residues Met173, Gly174, Tyr175, Pro191, Val195, and Leu199 define an equivalent hydrophobic patch on the surface of the UBA domain that is poised to interact with the Leu8-Ile44-Val70 hydrophobic patch on the ubiquitin surface (Figure 7B). Further, comparable intermolecular electrostatic interactions with Lys6 and Arg42 of ubiquitin are also possible, although these are likely to be mediated by UBA-1 Glu169 (with a slightly altered side chain conformation) and Glu196 mimicking CUE2-1 Asp18 and Asp40, respectively. The position occupied by UBA-1 Glu196 corresponds to that of CUE2-1 Gly44 (Figure 7A), which ,when mutated to an aspartate, increases the affinity of the interaction with ubiquitin relative to the wild-type protein. UBA-1 Ser172 may serve as an additional site of intermolecular interaction by engaging the His68 side chain of ubiquitin in a hydrogen bonding interaction.

A UBA surface similar to the one described above was previously predicted to interact with ubiquitin based on structural and mutational analyses (Bertolaet et al., 2001; Mueller and Feigon, 2002; Wilkinson et al., 2001). However, in the absence of a detailed model for the UBA-ubiquitin interaction, only two of the residues selected for the mutational analyses were from the putative ubiquitin binding site. In accord with our model, individual mutations of the conserved glycine residue in loop-1 and the second leucine in the dileucine motif near the carboxy terminus (Figure 7A) both compromised ubiquitin binding (Bertolaet et al., 2001; Wilkinson et al., 2001).

Functional Implications of Ubiquitin Recognition

A noteworthy feature of interactions involving monoubiquitin that have been described thus far, including the CUE2-1-ubiquitin interaction in this study, is the modest affinity (i.e., K_D 10–300 μM) of these interactions (Bertolaet et al., 2001; Raiborg et al., 2002; Shekhtman and Cowburn, 2002). The transient nature of the interaction implied by the low affinity therefore suggests that the monoubiquitin signal may be optimized for rapid dissociation from interacting partners. For example, components of the endocytic machinery are monoubiquitinated in addition to the cargo itself, and ubiquitin binding motifs are found in multiple proteins involved in various stages of the endocytic pathway (Donaldson et al., 2003; Hicke, 2001; Shih et al., 2003). Many interactions among

endocytic proteins that assemble to promote vesicle budding are of low affinity and may be cooperative, as most of these proteins bind to multiple partners. Transient association of ubiquitin with its binding domains may facilitate the dynamic assembly necessary to recruit cargo and form a budding vesicle. Transient interactions with ubiquitin and ubiquitin binding domains may also assist in transfer of monoubiquitinated cargo through the endocytic pathway in a temporally efficient manner.

A key question in monoubiquitin signaling concerns the maintenance of the signal in the cell—specifically, how is the addition of monoubiquitin versus a polyubiquitin chain regulated? In proteins that undergo intramolecular ubiquitination dependent on a UIM (or CUE) domain, it has been suggested that the ubiquitin binding domain interacts with the ubiquitin conjugated in *cis* to prevent extension of a ubiquitin chain (Polo et al., 2002; Shekhtman and Cowburn, 2002). In the CUE2-1-ubiquitin NMR structure, the ubiquitin surface contacted by the CUE domain extends to Lys48, a key residue in polyubiquitin chain formation located at the edge of the ubiquitin β sheet. Access to the Lys48 side chain is greatly restricted in the complex, suggesting a simple occlusion mechanism for inhibition of polyubiquitin chain formation. Conceivably, a similar mechanism may function in other processes that rely on monoubiquitin signals.

Another important question relates to the specificity of ubiquitin interactions involving CUE and UBA—particularly, whether these domains bind preferentially to monoubiquitinated or polyubiquitinated substrates. Based on the NMR structure of the CUE2-1-ubiquitin complex, it appears likely that CUE and UBA domains would be capable of binding polyubiquitinated substrates. Although the ubiquitin Lys48 side chain is greatly protected in the complex, the ϵ amino group points in the general direction of the solvent. Thus, any covalent linkage involving this moiety is likely to be accommodated without appreciably perturbing the CUE/UBA-ubiquitin interaction. This is in accord with previous observations that CUE and UBA domains can bind polyubiquitin in vitro (Shih et al., 2003; Wilkinson et al., 2001). Indeed, for many of these domains, it remains to be established whether monoubiquitin or polyubiquitin is the bona fide target in vivo. The multiplicity of ubiquitin units in polyubiquitin chains can potentially result in cooperative interactions with ubiquitin binding domains. Cooperative mechanisms of ubiquitin binding may involve novel surfaces on polyubiquitin chains and ubiquitin binding domains. With a clearer understanding of the structural basis for ubiquitin recognition at the monomer level at hand, the stage is now set for addressing issues of cooperativity in polyubiquitin recognition.

Experimental Procedures

Expression and Purification of CUE2-1

The coding sequence of the yeast Cue2 amino-terminal CUE domain, corresponding to residues 6–54, was amplified via PCR and inserted into the pMCSG7 expression vector (Stols et al., 2002). The expression construct introduces a 22 residue sequence that contains a His_6-tag and a TEV protease recognition site at the amino terminus of the protein. *E. coli* BL21(DE3) cells harboring the vector were grown at 37°C in M9 minimal media and shifted to 20°C before induction. Protein expression was induced using 1 mM IPTG when A_{600nm} was ~0.7 and cells were harvested 20 hr thereafter. Cell pellets were suspended in 20 mM sodium phosphate buffer (pH 7.4) containing 0.5 M NaCl, 1 mM PMSF, 1 μM leupeptin, 1 mM pepstatin, and 0.1% Triton X-100, lysed via sonication, centrifuged, and the supernatant loaded onto a Ni^{2+} affinity column (Sigma). The protein was eluted using 20 mM sodium phosphate, 0.5 M imidazole buffer (pH 7.4) containing 500 mM NaCl, and the protein-containing fractions were purified further via reversed-phase HPLC using a C18 column and a mobile phase containing 80% acetonitrile and 0.1% trifluoroacetic acid. The identity of the protein was confirmed by electrospray ionization mass spectrometry (ESI-MS). A CUE2-1 sample uniformly labeled with ^{15}N and ^{13}C isotopes was produced as described above, except cells were grown in media containing ^{15}N-ammonium sulfate (Martek) and $^{13}C_6$-D-glucose (Isotec), respectively. The extent of isotope incorporation was determined by ESI-MS to be >95% for ^{15}N and >97% for ^{13}C. The nonnative 22 residue sequence introduced by the expression vector was not removed prior to either NMR or analytical ultracentrifugation studies.

Expression and Purification of Yeast Ubiquitin

E. coli BL21(DE3) cells bearing a pET-3a ubiquitin expression vector were grown at 37°C in M9 minimal media containing ammonium sulfate and D-glucose either enriched in ^{15}N and/or ^{13}C isotopes, respectively, or at natural abundance. Protein expression was induced at the same temperature using 1 mM IPTG when A_{600nm} was 0.8. Cells were harvested 5 hr after induction. The protein was purified following the procedure described previously (Beal et al., 1996) except for the addition of a reversed-phase HPLC step as the final step of the purification protocol. The identity and integrity of the protein was verified by ESI-MS. The level of isotope enrichment for ^{15}N- and ^{15}N,^{13}C-labeled ubiquitin was >97% for ^{15}N and >96% for ^{13}C.

CUE2-1-Ubiquitin Complex Generation and NMR Sample Preparation

CUE2-1-ubiquitin complexes of 1:1 stoichiometry were generated for NMR studies by titrating increasing amounts of unlabeled ubiquitin with ^{15}N,^{13}C-labeled CUE2-1 and separately, unlabeled CUE2-1 with ^{15}N,^{13}C-labeled ubiquitin. Protein concentrations were determined spectrophotometrically (Gill and von Hippel, 1989). The progress of the titration was monitored by recording one-dimensional (1D) ^1H and two-dimensional (2D) ^1H-^{15}N correlated spectra. Protein concentrations for NMR studies were 1 mM, and all samples contained 20 mM sodium phosphate buffer (pH 7.0) and 0.2% NaN_3.

NMR Spectroscopy

NMR data were acquired on a Varian Inova 600 MHz spectrometer at 25°C. NMR data processing and analysis were performed using Felix 98 or Felix 2000 software (Accelrys), incorporating additional tools for accelerated resonance and NOE assignment developed in-house (Radhakrishnan et al., 1999). Backbone and side chain ^1H, ^{15}N, and ^{13}C resonances for CUE2-1 and ubiquitin were assigned by analyzing three-dimensional (3D) HNCACB, C(CO)NH-TOCSY, HNCO, ^{15}N-edited TOCSY, and HCCH-COSY spectra (Bax and Grzesiek, 1993; Ferentz and Wagner, 2000). Aromatic side chain resonances were assigned from 2D (HB)CB(CGCD)HD, (HB)CB(CGCDCE)HE, and ^{13}C-double-half-filtered TOCSY spectra (Otting and Wüthrich, 1990; Yamazaki et al., 1993).

NMR Restraint Generation

Structures were calculated using ARIA (version 1.2) in combination with CNS (Brünger et al., 1998; Linge et al., 2003). A total of 3238 NOE restraints derived from 3D ^{15}N-edited NOESY (mixing time, τ_m= 70 ms), 3D aliphatic ^{13}C-edited NOESY (τ_m= 50 ms), 3D ^{13}C-filtered, ^{13}C-edited NOESY (τ_m= 100 ms) spectra (Zwahlen et al., 1997), and 2D ^{13}C-double-half-filtered NOESY (optimized for aromatic resonances; τ_m= 50 ms) spectra recorded separately for the ^{15}N,^{13}C-CUE2-1-ubiquitin, and ^{15}N,^{13}C-ubiquitin-CUE2-1 samples were used in the calculations. Intermolecular NOEs were assigned manually and were calibrated indirectly by calculating a scaling factor for the intensities of well-resolved peaks found in both ^{13}C-edited NOESY and ^{13}C-filtered, ^{13}C-edited NOESY spectra. These NOEs were as-

signed upper bounds of 3, 4, 5, and 6 Å. All other NOEs were calibrated and assigned iteratively and automatically by ARIA. These NOEs were checked manually for errors after the conclusion of the penultimate refinement cycle.

A total of 150 torsion angle restraints were used including 69 ϕ and 69 ψ restraints derived from an analysis of H^{α}, C^{α}, C^{β}, C', and backbone ^{15}N chemical shifts using TALOS (Cornilescu et al., 1999) and 12 χ^1 (bounds $\pm$ 30°) restraints for isoleucine, threonine, and valine residues derived from measured $^3J_{NC^{\gamma}}$, and $^3J_{C'C^{\gamma}}$ values (Bax et al., 1994). Backbone ϕ and ψ restraints were applied to residues with TALOS reliability scores of ten, and the bounds were set to three times the standard deviation of the predicted values.

Structures were calculated from extended conformations as the starting model. Structures were calculated with default settings for most parameters in the ARIA run.cns task file. The number of steps in the simulated annealing protocol was doubled for improved convergence. The final force constants for the distance and torsion angle restraints were set to 50 kcal mol^{-1} $Å^{-2}$ and 200 kcal mol^{-1} rad^{-2}, respectively. Twenty structures were computed at each iteration for the first seven iterations, and the seven best structures were considered for automatic NOE assignment. In the eighth and ninth (final) iterations, 40 and 80 structures were computed, respectively. The 20 best structures from the final iteration were selected for structural analysis.

Structures were analyzed using PROCHECK (Laskowski et al., 1996), HBPLUS (McDonald and Thornton, 1994), and CNS (Brünger et al., 1998). Structural similarity searches were performed using the DALI web server (Holm and Sander, 1993). Interfacial surface areas were computed using MSMS (Sanner et al., 1996). Molecular images were generated using RIBBONS (Carson, 1997) and GRASP (Nicholls et al., 1991).

Analytical Ultracentrifugation

Purified CUE2-1 protein samples ranging in loading concentrations from 5–550 μM in 20 mM sodium phosphate buffer (pH 7.0) containing 150 mM NaCl were used for sedimentation equilibrium experiments. Sedimentation equilibrium experiments were performed at 24,000, 31,000, 38,000, 45,000, and 50,000 rpm at 20°C on a Beckman Coulter XL-A analytical ultracentrifuge. Data were acquired at three different wavelengths, each at a different starting protein concentration. Global fits were performed using UltraScan software. Protein samples before and after these experiments looked identical on an SDS-PAGE gel.

CUE2-1-Ubiquitin Affinity Measurements

The equilibrium dissociation constant for the CUE2-1-ubiquitin complex was measured using NMR spectroscopy. A 0.75 mM ^{15}N-ubiquitin sample was titrated with increasing amounts of a concentrated stock of unlabeled CUE2-1. Chemical shift deviations were computed using the formula $\Delta_{av} = \sqrt{\{[(\Delta_{HN})^2 + (\Delta_N/5)^2]/2\}}$. Nonlinear regression assuming a single binding site was performed using the program XMGR, employing the fitting function $y(x) = b\{[(x+1+a) - \sqrt{((x+1+a)^2 - 4x)}]/2\}$, where y(x) is the observed deviation at molar ratio x, and a and b are the fitted parameters related to the dissociation constant and the chemical shift deviation at $x = \infty$, respectively.

Ubiquitin Binding Assays

Wild-type and mutant ubiquitin and CUE2-1 proteins were expressed in *E. coli* as GST- or His_6-fusion proteins, and the binding assays were performed as described previously (Shih et al., 2002, 2003). The bound proteins were eluted by boiling in sample buffer, resolved on an SDS-PAGE gel, and analyzed by Coomassie staining or Western blot using anti-GST antibodies.

Acknowledgments

We thank Kurt Swanson, Sam Seaver, and Ben Ramirez for discussions. The pET-3a and pMCSG7 vectors were generous gifts from Cecile Pickart (Johns Hopkins) and Frank Collart (Argonne National Laboratory), respectively. This work was supported by funds from the NIH to I.R. and L.H. C.M.D. was supported by an IMGIP predoctoral fellowship. We gratefully acknowledge the Lurie Comprehensive Cancer Center for supporting the Structural Biology Center at Northwestern and the Keck Biophysics Facility at Northwestern for access to instrumentation (www.biochem.northwestern.edu/Keck/keckmain.html).

Received: February 26, 2003
Revised: April 25, 2003
Accepted: April 29, 2003
Published: May 29, 2003

References

Bax, A., and Grzesiek, S. (1993). Methodological advances in protein NMR. Acc. Chem. Res. *26*, 131–138.

Bax, A., Vuister, G.W., Grzesiek, S., Delaglio, F., Wang, A.C., Tschudin, R., and Zhu, G. (1994). Measurement of homonuclear and heteronuclear J-couplings from quantitative J-correlation. Methods Enzymol. *239*, 79–105.

Beal, R., Deveraux, Q., Xia, G., Rechsteiner, M., and Pickart, C. (1996). Surface hydrophobic residues of multiubiquitin chains essential for proteolytic targeting. Proc. Natl. Acad. Sci. USA *93*, 861–866.

Bertolaet, B.L., Clarke, D.J., Wolff, M., Watson, M.H., Henze, M., Divita, G., and Reed, S.I. (2001). UBA domains of DNA damage-inducible proteins interact with ubiquitin. Nat. Struct. Biol. *8*, 417–422.

Biederer, T., Volkwein, C., and Sommer, T. (1997). Role of Cue1p in ubiquitination and degradation at the ER surface. Science *278*, 1806–1809.

Brünger, A.T., Adams, P.D., Clore, G.M., DeLano, W.L., Gros, P., Grosse-Kunstleve, R.W., Jiang, J.S., Kuszewski, J., Nilges, M., Pannu, N.S., et al. (1998). Crystallography & NMR system: a new software suite for macromolecular structure determination. Acta Crystallogr. D Biol. Crystallogr. *54*, 905–921.

Carson, M. (1997). Ribbons. In Macromolecular Crystallography, Part B (San Diego: Academic Press, Inc.), pp. 493–505.

Chau, V., Tobias, J.W., Bachmair, A., Marriott, D., Ecker, D.J., Gonda, D.K., and Varshavsky, A. (1989). A multiubiquitin chain is confined to specific lysine in a targeted short-lived protein. Science *243*, 1576–1583.

Chen, L., Shinde, U., Ortolan, T.G., and Madura, K. (2001). Ubiquitin-associated (UBA) domains in Rad23 bind ubiquitin and promote inhibition of multi-ubiquitin chain assembly. EMBO Rep. *2*, 933–938.

Conaway, R.C., Brower, C.S., and Conaway, J.W. (2002). Emerging roles of ubiquitin in transcription regulation. Science *296*, 1254–1258.

Cornilescu, G., Delaglio, F., and Bax, A. (1999). Protein backbone angle restraints from searching a database for chemical shift and sequence homology. J. Biomol. NMR *13*, 289–302.

Dieckmann, T., Withers-Ward, E.S., Jarosinski, M.A., Liu, C.F., Chen, I.S., and Feigon, J. (1998). Structure of a human DNA repair protein UBA domain that interacts with HIV-1 Vpr. Nat. Struct. Biol. *5*, 1042–1047.

Donaldson, K.M., Yin, H., Gekakis, N., Supek, F., and Joazeiro, C.A. (2003). Ubiquitin signals protein trafficking via interaction with a novel ubiquitin binding domain in the membrane fusion regulator, Vps9p. Curr. Biol. *13*, 258–262.

Ferentz, A.E., and Wagner, G. (2000). NMR spectroscopy: a multifaceted approach to macromolecular structure. Q. Rev. Biophys. *33*, 29–65.

Garcia-Higuera, I., Taniguchi, T., Ganesan, S., Meyn, M.S., Timmers, C., Hejna, J., Grompe, M., and D'Andrea, A.D. (2001). Interaction of the Fanconi anemia proteins and BRCA1 in a common pathway. Mol. Cell *7*, 249–262.

Gill, S.C., and von Hippel, P.H. (1989). Calculation of protein extinction coefficients from amino acid sequence data. Anal. Biochem. *182*, 319–326.

Hershko, A., and Ciechanover, A. (1998). The ubiquitin system. Annu. Rev. Biochem. *67*, 425–479.

Hicke, L. (2001). A new ticket for entry into budding vesicles-ubiquitin. Cell *106*, 527–530.

Hofmann, K., and Bucher, P. (1996). The UBA domain: a sequence motif present in multiple enzyme classes of the ubiquitination pathway. Trends Biochem. Sci. *21*, 172–173.

Hofmann, K., and Falquet, L. (2001). A ubiquitin-interacting motif conserved in components of the proteasomal and lysosomal protein degradation systems. Trends Biochem. Sci. *26*, 347–350.

Holm, L., and Sander, C. (1993). Protein structure comparison by alignment of distance matrices. J. Mol. Biol. *233*, 123–138.

Katzmann, D.J., Odorizzi, G., and Emr, S.D. (2002). Receptor downregulation and multivesicular-body sorting. Nat. Rev. Mol. Cell Biol. *3*, 893–905.

Klapisz, E., Sorokina, I., Lemeer, S., Pijnenburg, M., Verkleij, A.J., and van Bergen en Henegouwen, P.M. (2002). A ubiquitin-interacting motif (UIM) is essential for Eps15 and Eps15R ubiquitination. J. Biol. Chem. *277*, 30746–30753.

Laskowski, R.A., Rullmann, J.A., MacArthur, M.W., Kaptein, R., and Thornton, J.M. (1996). AQUA and PROCHECK-NMR: programs for checking the quality of protein structures solved by NMR. J. Biomol. NMR *8*, 477–486.

Lee, A.L., and Wand, A.J. (1999). Assessing potential bias in the determination of rotational correlation times of proteins by NMR relaxation. J. Biomol. NMR *13*, 101–112.

Linge, J.P., Habeck, M., Rieping, W., and Nilges, M. (2003). ARIA: automated NOE assignment and NMR structure calculation. Bioinformatics *19*, 315–316.

McDonald, I.K., and Thornton, J.M. (1994). Satisfying hydrogen bonding potential in proteins. J. Mol. Biol. *238*, 777–793.

Mueller, T.D., and Feigon, J. (2002). Solution structures of UBA domains reveal a conserved hydrophobic surface for protein-protein interactions. J. Mol. Biol. *319*, 1243–1255.

Muratani, M., and Tansey, W.P. (2003). How the ubiquitin-proteasome system controls transcription. Nat. Rev. Mol. Cell Biol. *4*, 192–201.

Nicholls, A., Sharp, K.A., and Honig, B. (1991). Protein folding and association: insights from the interfacial and thermodynamic properties of hydrocarbons. Proteins *11*, 281–296.

Oldham, C.E., Mohney, R.P., Miller, S.L., Hanes, R.N., and O'Bryan, J.P. (2002). The ubiquitin-interacting motifs target the endocytic adaptor protein epsin for ubiquitination. Curr. Biol. *12*, 1112–1116.

Otting, G., and Wüthrich, K. (1990). Heteronuclear filters in two-dimensional [^{1}H,^{1}H]-NMR spectroscopy: combined use with isotope labelling for studies of macromolecular conformation and intermolecular interactions. Q. Rev. Biophys. *23*, 39–96.

Pickart, C.M. (2001). Mechanisms underlying ubiquitination. Annu. Rev. Biochem. *70*, 503–533.

Polo, S., Sigismund, S., Faretta, M., Guidi, M., Capua, M.R., Bossi, G., Chen, H., De Camilli, P., and Di Fiore, P.P. (2002). A single motif responsible for ubiquitin recognition and monoubiquitination in endocytic proteins. Nature *416*, 451–455.

Ponting, C.P. (2000). Proteins of the endoplasmic-reticulum-associated degradation pathway: domain detection and function prediction. Biochem. J. *351*, 527–535.

Pornillos, O., Garrus, J.E., and Sundquist, W.I. (2002). Mechanisms of enveloped RNA virus budding. Trends Cell Biol. *12*, 569–579.

Radhakrishnan, I., Perez-Alvarado, G.C., Parker, D., Dyson, H.J., Montminy, M.R., and Wright, P.E. (1999). Structural analyses of CREB-CBP transcriptional activator-coactivator complexes by NMR spectroscopy: implications for mapping the boundaries of structural domains. J. Mol. Biol. *287*, 859–865.

Raiborg, C., Bache, K.G., Gillooly, D.J., Madshus, I.H., Stang, E., and Stenmark, H. (2002). Hrs sorts ubiquitinated proteins into clathrin-coated microdomains of early endosomes. Nat. Cell Biol. *4*, 394–398.

Rotin, D., Staub, O., and Haguenauer-Tsapis, R. (2000). Ubiquitination and endocytosis of plasma membrane proteins: role of Nedd4/Rsp5p family of ubiquitin-protein ligases. J. Membr. Biol. *176*, 1–17.

Sanner, M.F., Olson, A.J., and Spehner, J.C. (1996). Reduced surface: an efficient way to compute molecular surfaces. Biopolymers *38*, 305–320.

Shekhtman, A., and Cowburn, D. (2002). A ubiquitin-interacting motif from Hrs binds to and occludes the ubiquitin surface necessary for polyubiquitination in monoubiquitinated proteins. Biochem. Biophys. Res. Commun. *296*, 1222–1227.

Shih, S.C., Katzmann, D.J., Schnell, J.D., Sutanto, M., Emr, S.D., and Hicke, L. (2002). Epsins and Vps27p/Hrs contain ubiquitin-binding domains that function in receptor endocytosis. Nat. Cell Biol. *4*, 389–393.

Shih, S.C., Prag, G., Francis, S.A., Sutanto, M.A., Hurley, J.H., and Hicke, L. (2003). A ubiquitin-binding motif required for intramolecular monoubiquitylation, the CUE domain. EMBO J. *22*, 1273–1281.

Sloper-Mould, K.E., Jemc, J.C., Pickart, C.M., and Hicke, L. (2001). Distinct functional surface regions on ubiquitin. J. Biol. Chem. *276*, 30483–30489.

Stols, L., Gu, M., Dieckman, L., Raffen, R., Collart, F.R., and Donnelly, M.I. (2002). A new vector for high-throughput, ligation-independent cloning encoding a tobacco etch virus protease cleavage site. Protein Expr. Purif. *25*, 8–15.

Thrower, J.S., Hoffman, L., Rechsteiner, M., and Pickart, C.M. (2000). Recognition of the polyubiquitin proteolytic signal. EMBO J. *19*, 94–102.

Vijay-Kumar, S., Bugg, C.E., and Cook, W.J. (1987). Structure of ubiquitin refined at 1.8 Å resolution. J. Mol. Biol. *194*, 531–544.

Weissman, A.M. (2001). Themes and variations on ubiquitylation. Nat. Rev. Mol. Cell Biol. *2*, 169–178.

Wilkinson, C.R., Seeger, M., Hartmann-Petersen, R., Stone, M., Wallace, M., Semple, C., and Gordon, C. (2001). Proteins containing the UBA domain are able to bind to multi-ubiquitin chains. Nat. Cell Biol. *3*, 939–943.

Yamazaki, T., Forman-Kay, J.D., and Kay, L.E. (1993). 2-dimensional NMR experiments for correlating $^{13}C^{\beta}$ and $^{1}H^{\delta/\epsilon}$ chemical-shifts of aromatic residues in ^{13}C-labeled proteins via scalar couplings. J. Am. Chem. Soc. *115*, 11054–11055.

Young, P., Deveraux, Q., Beal, R.E., Pickart, C.M., and Rechsteiner, M. (1998). Characterization of two polyubiquitin binding sites in the 26 S protease subunit 5a. J. Biol. Chem. *273*, 5461–5467.

Zwahlen, C., Legault, P., Vincent, S.J.F., Greenblatt, J., Konrat, R., and Kay, L.E. (1997). Methods for measurement of intermolecular NOEs by multinuclear NMR spectroscopy: application to a bacteriophage lambda N-peptide/boxB RNA complex. J. Am. Chem. Soc. *119*, 6711–6721.

Accession Numbers

The PDB accession code for the NMR ensemble is 1OTR.